2

Conf-9408127--4

UCRL-JC-118127
PREPRINT

Hohlraums Energy Balance and X-Ray Drive

J. D. Kilkenny

This paper was prepared for inclusion in a book collection from the
Scottish Universities Summer School in Physics
St. Andrews, Scotland
August 7-12, 1994

August 4, 1994

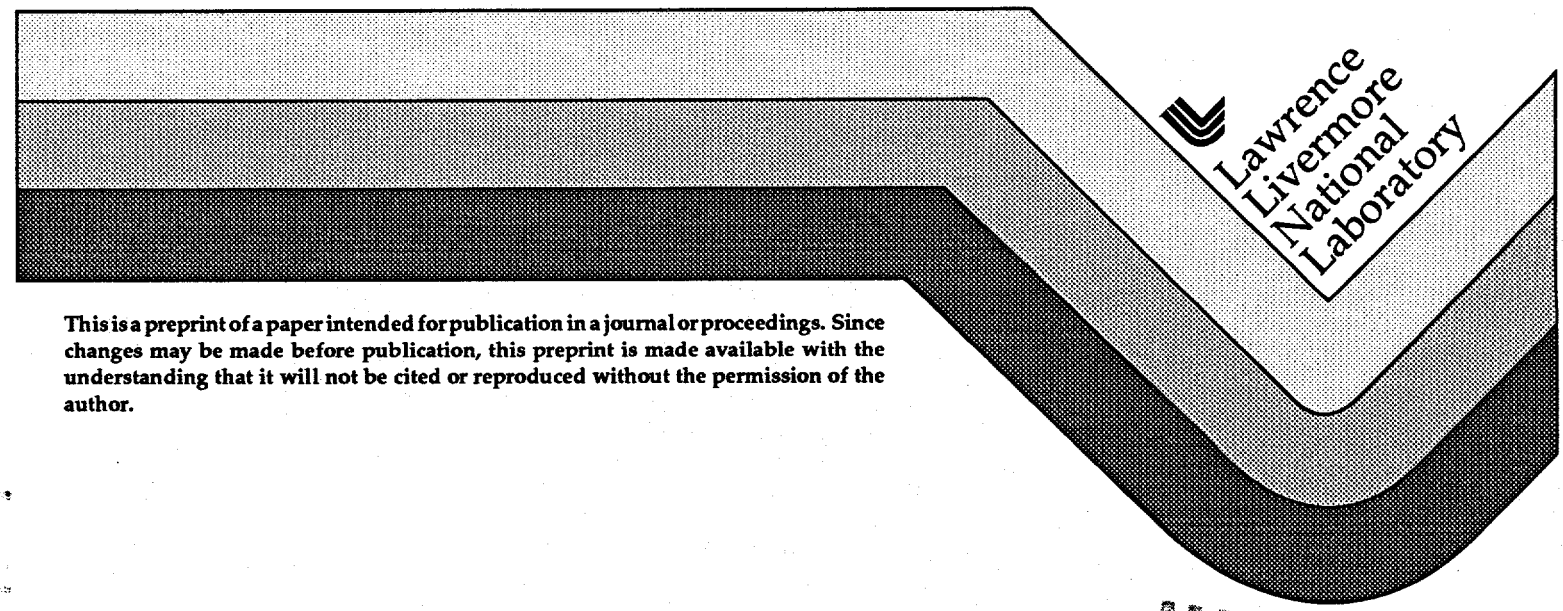

875

DISCLAIMER

Portions of this document may be illegible in electronic image products. Images are produced from the best available original document.

2. Hohlraums Energy Balance and X-Ray Drive

For many years there has been an active ICF program in the U.S. concentrating on x-ray drive. X-ray drive is produced by focusing laser beams into a high Z hohlraum. Conceptually, the radiation field comes close to thermodynamic equilibrium, that is it becomes isotropic and Planckian. These properties lead to the benefits of x-ray drive—it is relatively easy to obtain drive symmetry on a capsule with no small scalelengths drive perturbations. Other advantages of x-ray drive is the higher mass ablation rate, leading to lower growth rates for hydrodynamic instabilities (see Section 3). X-ray drive has disadvantages, principally the loss of energy to the walls of the hohlraum.

2.1 Review of Black Body Radiation

First, let us review the properties of black-body radiation. The Planckian or black body spectral intensity, the power/bandwidth/solid angle, is:

$$I_{\nu p}(\nu) = \frac{c\rho_{\nu p}}{4\pi} = \frac{2h\nu^3}{c^2}\,\frac{1}{\exp(h\nu/kT)-1}$$

where $\rho_\nu p$ is the radiation energy density/bandwidth. The peak of $I_{\nu p}$ or $\rho_{\nu p}$ occurs at $h\nu_{max} = 2.8\,kT$. Note that $I_\lambda\, d\lambda = I_\nu d_\nu$. The black body spectral intensity is isotropic and so the net power flux through a surface is zero. However, the one-sided flux

$$F_p = \int_o^\infty \int_{2\pi} I_{\nu p} \cos\theta \; d\Omega d\nu = \sigma T^4$$

Work performed under the auspices of the DOE by LLNL under contract no. W-7405-Eng-48.

where σ is the Stefan-Boltzmann constant. In units useful for ICF, $\sigma = 1.03\ 10^5$ $W/cm^2/eV^4$. ICF needs radiation temperatures in the range 200-300 eV leading to an inward flux onto a capsule σT^4 of 1.6×10^{14} W/cm^2 - 8×10^{14} W/cm^2, giving ablation pressures in the regime 100 Mbar.

The Planckian radiation energy density is $\rho_p = 4\pi\sigma T^4/c$. At 200 eV this is only $5\ 10^4$ J/cm^3—much less than the matter energy density at normal densities: although the energy density is low, the high velocity of light makes it effective or dominant for energy transport.

2.2 Laser absorption and conversion to x-rays

When high power laser light is incident on a solid surface and the power absorption exceeds the heat flow- occurring at $I > 10^{10}$ W/cm^2, the solid heats, vaporizes and becomes a plasma. At this stage, the surface becomes a conventional laser plasma with processes illustrated in Fig. 1. Laser or x-ray energy, incident from the left, passes through the "ablating" plasma that has a scale length L determined by the energy absorption process. For radiation of frequency ω, the refractive index are

$$n_r^2 = (1 - \omega_p^2/\omega^2)$$

$$\text{where } \omega_p^2 = 4\pi ne^2/m_e$$

Laser propagation occurs until $\omega p > \omega$ or put another way unit the laser beam reaches the critical (electron) density n_c for its wavelength which in practical units is $n_c = 10^{21} / \lambda^2$ cm-3 where λ is in μm. For densities close to the critical density, the absorption coefficient, which is inverse bremsstrahlung absorption, become high. The absorption length is

$$L = V_g/\nu_{ei} \times (n/n_c)$$

where V_g is the group velocity and ν_{ei} is the electron ion collision frequency. For example, at $n = n_c/2$, in Z = 2 or Z = 50 at T = 3 keV and 0.35 μm light L = 0.8 and 0.3 mm respectively, that is absorption by inverse Bremsstrahlung can becomesvery high close to the critical density.

Real physical phenomena can be far more complex. The process determining the scale length of energy transport are complex, and inverse bremsstrahlung (i.b.) can have a different functional form in tenuous plasmas and i.b. can be augmented by many other plasma processes - see Kruer's talk (1).

Sets of measurements of the plasma absorptions at different laser wavelengths and pulse lengths are materials were carried out in the late seventies and eighties (2), and are summarized in Figure 2. There are several trends

- higher intensity, leads to higher T and lower absorption because L increases
- longer pulse length gives more absorption because of the increase in L
- higher Z material is more absorptive

From the point of view of ICF, with L~mm, high Z material and T ~ keV, the absorption fraction is high, i.e. $\eta_{abs} \geq 90\%$. (There is a rather different field of laser-matter interactions using short pulse lasers where intensities exceeding 10^{18} W/cm^2 in sub-picosecond pulses leads to field ionization of matter - this is the subject of Bingham's lectures)(3).

The conversion of laser light to x-rays can be globally written as

$$I_{x\text{-}ray} = \eta_{xa} \times \eta_{abs} I_{inc}$$

where η_{xa} is the conversion efficiency of the absorbed flux to x-rays. The phenomena determining the values of η_{xa} are complex - they involve an accurate description of atomic physics, radiation transfer as well as the laser absorption processes. An accurate

detailed description has not yet been made, however the basic physics is understood well enough to account for the observed trends.

The black body curve is usually a reference point. If the plasma is optically thick at all frequencies, it will radiate like a black body. The peak of the spectrum will be at $h\upsilon \sim 3kT$ and the power will be σT^4. The key is the "opacity" τ of the material where $\tau(\upsilon) = \int \kappa_\upsilon(\upsilon)\, dx$ and κ_υ is the absorption coefficient. There are two principal contributors to κ, continuum and line absorption. The details will be examined in Sigel's lectures, but are succinctly illustrated in Figure 3 representing the radiation transfer equation for a planar slab. For low opacity, $\tau < 1$ at all frequencies, the spectrum emitted by a plasma is just the lines, with no reabsorption of the line emission in the medium. As the absorption increases, the opacity at line center starts to exceed 1, i.e. $\tau_{\text{line center}} > 1$. Photons at this frequency are absorbed, but then remitted. Detailed balance of the processes starts to occur and the radiation is described by the black body curve, but only at this frequency. The spectrum then has optically thick lines with the tops of the lines described by the black body spectrum, $I_{\upsilon p}$. Then as the thickness of the plasma further increases, so that $\tau > 1$ becomes true at all frequencies the emission comes up to $I_{\upsilon p}$ at all frequencies. This thought experiment is illustrative but assumes that the atomic levels are kept in local thermodynamic equilibrium (l.t.e.) with no temperature gradients. Real plasmas are not so cooperative!

To achieve a high x-ray conversion efficiency in a plasma, the opacity and temperature of the plasma should both be high. The absorption coefficients, of both continuum absorption and line absorption both increases with Z of the material. For hydrogen like plasmas, the bound-free absorption cross section is

$$\sigma_{\upsilon n} = 8 \times 10^{-18} \frac{n_e}{Z^2} \left(\frac{\nu_n}{\nu}\right)^3 \text{ cm}^2$$

For cold material, the cold x-ray absorption coefficients for gold and carbon are shown in Figure 4. Here the values of f_2, related to μ are plotted so that the x-ray absorption is

$$I = I_0 \exp(-\mu)$$

where ρ and t are the density and thickness of the absorber.

The bound-free absorption cross n is the quantum number of the initial state of the hydrogen like atom of charge Z, and $h\upsilon_n = I_H Z^2/n^2$, the minimum energy of a photon required to photoionize an atom with an electron in level n.

Both extreme examples show that as the Z of matter increases, the opacity increases.

Extensive experimental measurements have been made of the overall x-ray conversion efficiency from laser light to x-rays for gold targets. For open geometry targets, the conversion efficiency is shown in Figure 5. It ranges from 60-80% at 10^{14} W/cm^2 for 0.35 μm light to 45-60% at 10^{15}W/cm^2. The conversion efficiency has been measured to be higher for limited mass targets, being ~70% for small gold spheres. For small targets, there is less opportunity for sideways loss of energy into surrounding cold material.

The measured time dependence of the x-ray conversion efficiency, η_x is shown in Figure 6. It is clearly seen that as t increases, so does η_x because the size of the plasma cloud forming in front of the solid surface increases - there is a corresponding increase in τ, η_{abs} and T. In hohlraums, we will see that η_x can be even higher. This is because of several effects, summarized by the reduced losses of energy into other channels, particularly hydrodynamic expansion losses.

2.3 The x-ray absorption coefficient in matter and Rosseland mean free path

The continuum absorption cross section for bound-free transitions in a hydrogen like plasma, leads to a sawtooth absorption cross section resulting from absorption occurring when the photon energy exceeds photo-ionization energies for atoms in different ionization levels and different states of ionization within a state of ionization. By summing over the various states, with thermal population of the states absorption coefficients for bound-free absorption can be derived and are of a form

$$K_\nu = K_1 \frac{Z^4}{\upsilon^3} n_e$$

Zeldovich and Raiser (4) also point out that for $h\nu > kT$, a situation common in radiation transport as the black body peaks at ~3kT, and the Rosseland mean averages at 4-5 kT, bound-free continuum absorption is usually dominant because the ratio of bound-free/free-free $\alpha (\exp(h\upsilon/kT)^{-1})$

Both the bound-free hydrogen like and the bound-free cold absorption coefficients exhibit a υ^{-3} dependence above threshold, arising from the density of states.

The cold absorption cross section shows the various levels of the cold atom. Carbon and goldare illustrated in Figure 4. The M shell (n = 3) and N shell (n = 4) edges are notable for Au and are relevant to ICF. The complexity of the atomic structure of Au can be seen from the cold absorption. The M edge is actually five edges (the L edge is three). For ionized matter, the absorption coefficients change and become more complex because there are many states of ionization existing at the same time even with no gradients in temperature. Furthermore, the high temperature ionizes the atoms, opening up the full shells of cold material and allowing many bound-bound transitions. For high Z atoms, most of these transitions are "unresolved" and unresolved transition arrays - UTA form with high opacity.

For the absorption as a function of frequency, the radiation mean free path $\ell_\nu{}^1$(m.f.p.) as a function of frequency can be obtained. For energy transport, an average radiation m.f.p. is relevant. The most relevant average is the Rosseland mean.

As in any diffusion process, the energy flux at a particular frequency is

$$\underline{S}_\upsilon = - \ell_\upsilon{}^1 c/3 \ \nabla \rho_{\upsilon p}$$

The total flux is

$$\underline{S} = -c/3 \int_o^\infty \ell_\upsilon{}^1 \ \nabla \rho_{\upsilon p} \, d\upsilon$$

As $\int_o^\infty \rho_{\upsilon p} \, d\upsilon = 4 \sigma T^4/c$,then, $\underline{S} = -\ell_R \, c/3 \ \nabla \rho_\upsilon = -16/3 \ \sigma \lambda_R T^3 \ \nabla T$

where λ_R is the Rosseland averaged m.f.p.

It can be shown (4), that λ_R is the spectral integral of $\ell_\upsilon{}^1$ with a weighting factor $x^4 e^{-x} / (1-e^{-x})^2$, which has a maximum at ~4kT, sand so the high energy photons are dominant in energy transfer.

The equation for the radiant energy flux (in l.t.e.) has a coefficient times a temperature gradient, similar to a thermal conductivity times a temperature gradient for heat flow. By analogy, the coefficient of thermal conductivity is $16/3 \, \sigma \ell T^3$. The strong dependence on T, leads to a very non-linear, flat topped radiation wave.

2.4 Marshak waves in high Z material

The generalized energy flow equation is d/dt (energy density) = -d/dx (energy flux). A normal conduction wave results if the energy density is stored in specific heat of matter and the energy flux is by heat flow. For pure radiation waves, the energy flow would be by radiation and the energy density would be in the radiation energy density $\rho \approx$

$4\sigma T^4/c$. But for temperatures of interest to ICF, the radiation energy density is much less than the matter energy density and so the energy flow equation is d/dt (matter energy density) = -d/dx (radiant energy flux).

The impact of this is to slow down the radiation wave so that the diffusivity L^2/T instead of being $c\lambda_R/3$ as one would expect is reduced to $C\lambda_R/3$ x (radiation energy density/matter energy density). More exactly

$$d\varepsilon_{th}/dt = -d/dt\,(-16/3\sigma\lambda_R T^3\ dT/dx).$$

The thermal energy $\varepsilon_{th} \alpha\ T^{1.5}$ (this is ZnkT, $\frac{3}{2} = n_e kT$ and the state of ionization is determined approximately by $Z^2 E_H \sim kT/3$).

This is essentially a diffusion equation. The diffusivity $\frac{L^2}{T} \sim c\lambda_R/2$ x ratio of energy densities. Where L is the characteristic penetration depth of the heat front. As $\lambda_R \sim T^{1.5}/K_0$ where K_0 is a characteristic absorption of the material, then $L \sim t^{0.5} T^2 / \sqrt{\kappa_0}$

Using cold values for opacity then at say 200 eV and 1 nsec for gold L~ 1 μm.

This is a very oversimplified treatment. The hydrodynamic response of the material has been omitted. The surface ablates and a shock wave would be driven into the material. The Marshak (radiation) wave is at low temperatures slower than the shock wave. The shock wave can be used to measure the temperature as discussed below, and in this application, the shockwave goes much faster than the radiation wave. The transition temperature when the radiation wave outruns the shock wave is discussed elsewhere.

Measurements of the velocity of the Marshak wave have been made by observing with a soft x-ray instrument the break-out of the wave through different thicknesses of

gold[5]. Typical data for Nova experiments is shown in Figure 6, together with the burnthrough time for various thicknesses of material. There is good agreement with detailed Lasnex modeling. The surprising feature of Figure 6 is the constant velocity of propagation of the Marshak wave, because for constant T, $dL/dt \propto t^{-0.5}$. However, as discussed in Zeldovich and Raiser[4], the constant velocity results form the energy flux into the material not being constant, because the laser power is flat topped, and in this situation the drive temperature rises.

2.5 X-ray albedo

The x-ray albedo defined as

$$\alpha = \frac{\text{x-ray flux emitted by the surface}}{\text{x-ray flux incident on a surface}}$$

is a useful parametrization for hohlraums and Marshak waves. If the incident reradiated and absorbed fluxes are S_i, S_r and S_{abs} respectively then

$$S_i - S_r = S_{abs} \sim \varepsilon \dot{L} \sim T^{1.5}\ T^2/t^{0.5}$$

$$\alpha = S_r/S_i = \alpha\sigma T^4/(\alpha\sigma T^4 + K_1 T^{3.5}/t^{0.5})$$

Where K_1 is constant

$$\therefore \alpha = 1/(1 + K_1/T^{0.5}\ t^{0.5})$$

That is there is a weak temperature and time dependence to α. As T and t increase the value of α comes closer to one. From Sigel's data[5], the derived value for α for gold at 1 nsec varies from $\alpha = 0.75$ to $\alpha = 0.85$ as T increases from 150 eV to 250 eV.

2.6 Power balance and hohlraum temperature

The radiation temperature in a hohlraum is determined by a balance of sources and sinks as illustrated in Figure 8. The x-ray source is ηP_L where P_L is the laser power, the hole loss is $\sigma T^4 A_h$, and the wall loss is $(1-\alpha)\ \sigma T^4 A_w$, where A_h and A_w are the areas of

the hole and wall respectively, and T is the effective brightness temperature of the hohlraum.

In balance, $\eta P_L = (A_w (1-\alpha) + A_h)\ \sigma T^4$

This equation quite accurately describes the temperatures measured on Nova hohlraums. The key parameters are α and η. For Nova hohlraums, α is effectively measured by the radiation burnthrough experiments. The other parameter η has been measured with open geometry experiments, and for Nova hohlraums experiments, higher values are found.

Experiments have been performed using the Nova laser to measure drive scaling and laser coupling in cavity targets used for implosions and other radiation heating experiments. Targets are right circular cylinders of high Z material, typically Au. Ten Nova beams, five per side, are focused through laser entrance holes (LEH) in the ends of the cylinders onto the cylinder walls. Cavities are heated with as much as 30 TW of 0.35 μm light in a 1 ns square laser pulse or with shaped pulses as long as 3.7 ns with up to 40 kJ of laser energy. Average intensity on the cavity wall is ~1×10^{15} W/cm^2 for 30 TW pulses. Scaling is investigated using 1.2 mm and 1.0 mm diameter targets whose other dimensions are scaled appropriately.

The radiation temperature, T_R, in the cavities is determined using two independent methods. One method measures T_R by observing the velocity of a shock wave generated when radiation is absorbed in low Z material, typically Al. T_R can be correlated to the shock velocity , u_s, using strong shock relations ( ). For low Z materials, the hot ablated plasma is relatively transparent to the x-rays while the cold material is very absorptive establishing a short heat front. The heat front is sub-sonic and establishes a shock wave ahead of it. The shock velocity scales approximately as u_s

α $T_R 7/4$ with the proportionality constant depending on the equation of state. A slight correction to the temperature scaling is needed for the reradiation of Al. For the temperature range of these experiments, the scaling is $T_R = 0.0126\ u_s^{0.63}$ where T_R is in units of eV and u_s is in units of cm/s.

The shock velocity is measured by placing an Al plate over a hole in the cavity. Its thickness is continuously varied, as shown schematically in Figure 9a, or varied in discrete steps. Optical emission is produced when the radiation generated shock wave emerges from the rear surface. The optical emission is imaged onto the slit of an optical streak camera using an f/10 Cassegrain telescope. An example of data is shown in Figure 9b for a laser heating pulse 2.2 ns long with a 3:1 contrast. The onset of optical emission as a function of time is extracted and correlated with the initial Al thickness as shown in Figure 9c. Estimated error for measuring drive is $\pm$ 5 eV which includes the accuracy of the measurement and the uncertainty in the shock scaling.

The other method measures the reradiated flux, S_r, from the x-ray heated wall similar to previous cavity characterization experiments. The flux is measured using an array of x-ray diodes[7] through a Be-lined hole in the hohlraum wall placed so that the diodes view only unirradiated wall. Time resolution is on the order of 150 ps limited by the bandwidth of the detectors and oscilloscopes and correlation of the timing among the detectors. Spectrally integrated flux is measured to an accuracy of ~25% including calibration errors and unfolding uncertainties resulting in ±6% when converted to an equivalent radiation temperature using the Stefan-Boltzmann law.

Scaling experiments have been performed using 1 ns constant power (square) laser pulses. Scaling of T_R as a function of average laser power is shown in Figure 10 for 1.6 mm diameter cavities as measured form the shock breakout. Most data are from targets

2.55 mm long although some data from longer targets are included. Small corrections (<5 eV) have been made to these data for comparison. T_R is around 270 eV for 30 TW of incident laser power. In limited experiments with smaller cylindrical cavities, we measure temperatures of 290 eV and 300 eV for a 1.2 mm and 1.0 mm diameter cavity, respectively. These data are also shown in Fig. . For the 1.0 mm diameter cavity, the laser entrance holes were larger so that the fraction of hole area is increased to 11% vs. 6% for the larger targets. Previous experiments have reported temperatures of 240 eV using 1 mm dia. spherical cavities heated with 5.5 TW of 0.35 μm light using the GEKKO laser at Osaka. The present experiments significantly extend the range of radiation temperatures attained in the laboratory to temperatures of interest for high gain implosions.

The data in Figure 10 can be fit by eq. using the radiation heating model of high Z walls by Sigel, et al.[8] with the fitting parameter is η. Results of the fit are the lines shown in Figure 10 with η being 0.75, 0.65, and 0.50 for the 1.6 mm, 1.2 mm and 1.0 mm diameter cavities, respectively. Standard deviations of the fits are ± 0.1, consistent with measurement accuracy for laser power and T_R. The fit for the 1.6 mm cavities follow the trend of the data quite well demonstrating the scaling with the simple power balance model.

The 1.6 mm cavities have been modeled using 2-D LASNEX, a radiation hydrodynamics simulation code including treatment of the laser rays and energy deposition. Results of the calculations are also shown as open circles in Fig. In general, the modeling results agree with the experiment indicating that the calculations are predicting laser deposition, x-ray conversion, x-ray absorption by the wall, and reradiation correctly. The agreement also supports predictions for extrapolation to high gain targets which use the same modeling.

For high gain implosions, the driving pulse is ramped to reduce shock preheating of the fuel before compression. We have generated a number of high contrast, shaped radiation pulses on Nova for a variety of experiments simply by varying the temporal profile of the incident laser pulse. Previous experiments have reported results using only simple quasi-Gaussian laser pulses. An example of a shaped radiation pulse measured is shown in Fig. along with the incident laser power. The incident laser pulse is 2.2 ns long with a 3:1 contrast ratio from the start of the pulse to its peak. The resulting reradiated brightness temperature, $(S_r/\sigma)^{1/4}$, is 135 eV in the initial part of the pulse with a peak of 200 eV, or a flux (σT_R^4) contrast of ~4. Other tailored pulses have been successfully demonstrated on Nova with pulses as long as 3.7 ns. As the pulse length increases, energy limits on Nova restrict the peak temperatures available. The ease of obtaining shaped laser pulses allows a significant flexibility in optimizing implosion experiments.

In general, x-ray drive becomes easier for larger facilities, because the temperature is determined by the wall loss $1-\alpha \sim 1/T^{0.5}\, t^{0.5}$. For longer times, or for higher temperatures, the wall loss drops. For Nova, t ~ 1 nsec, T ~ 260 eV and $1 - \alpha = 0.2$: in contrast the NIF will have t ~ 10 nsec and T ~ 300 eV and $1 - \alpha \sim 0.11$, as illustrated in table

	P_L(TW)	ηP_L	$(1-\alpha)\, A_w$(mm²)	$A_h$mm²	T_eV
Nova	30	22	0.2 x 16	12	260
NIF	470	380	0.1 x 200	12	300

Table Comparison of source and sink terms for Nova and NIF

References II

(1) W. Kruer, ibid.

(2) Absorption measurements.

(3) R. Bingham, ibid.

(4) Y. Zeldovich and Y. Raiser, Physics of Shock Waves and High Temperature Hydrodynamic Phenomena: Academic Press, New York 1966.

(5) R. Sigel, et.al., Phys. Rev. A 38, 5779 (1988).

(6) S.P. Hatchett, Lawrence Livermore National Laboratory Report No. UCRL-JC-108348, 1991 (unpublished; available through National Technical Information Service, ref. #DE 92006882).

(7) H.N. Kornblum, R.L. Kauffman, and J.A. Smith, Rev. Sci. Instrum. 57, 2179 (1986).

(8) R. Sigel, R. Pakula, S. Sakabe, and G.D. Tsakiris, Phys. Rev. A. 38, 5779 (1988).

A laser heats the plasma, causing a rocket blow off and driving a shock into high density material

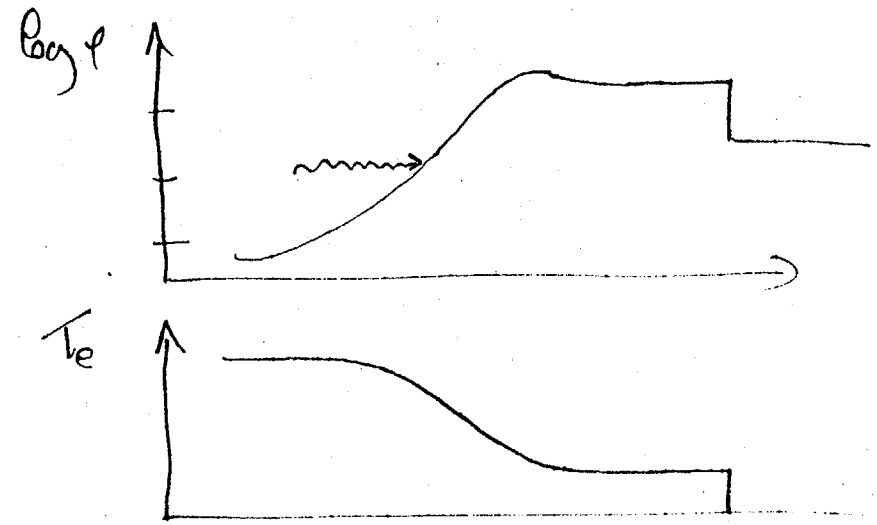

Kathy I will draw in

Fig 1

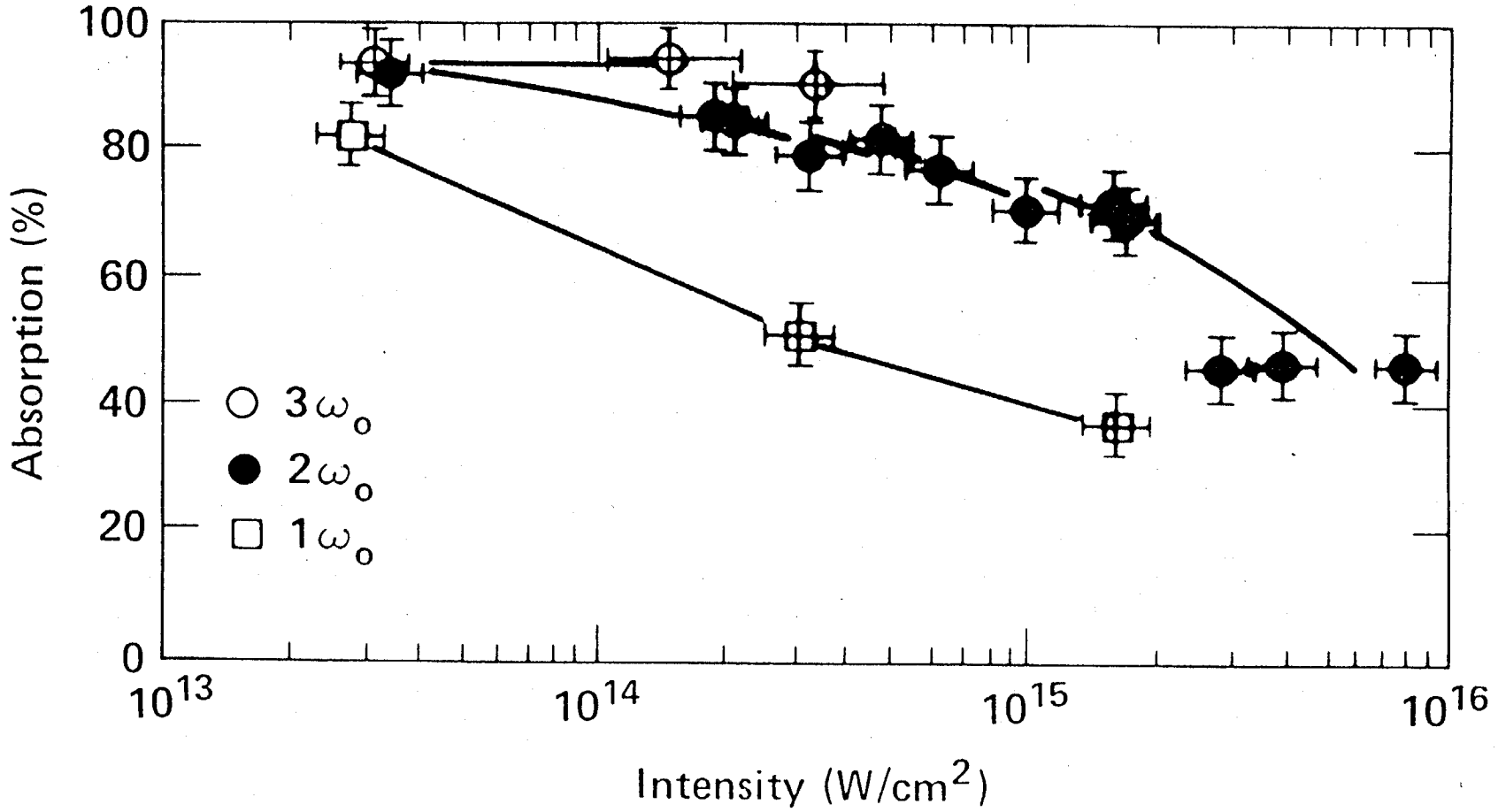
100
80
60
40
20
0
Absorption (%)
3ω_o
2ω_o
1ω_o
10^13
10^14
10^15
10^16
Intensity (W/cm^2)

Figure 2

As the length ℓ of a plasma is increased the emission approaches the black-body limit - first on lines, then in the continuum

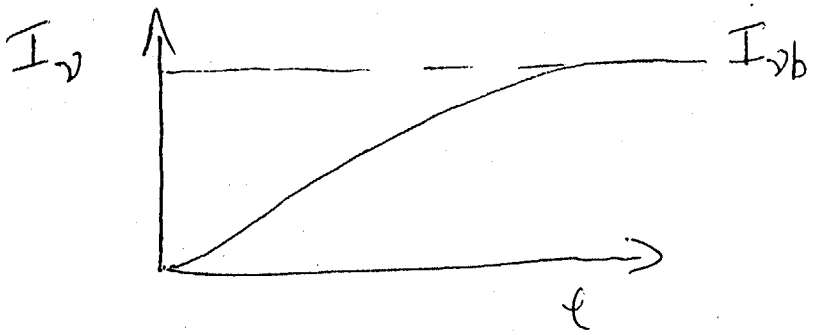

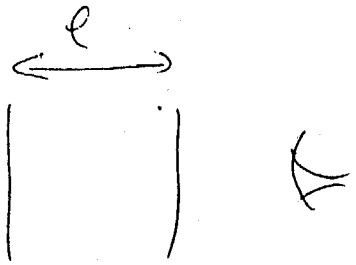

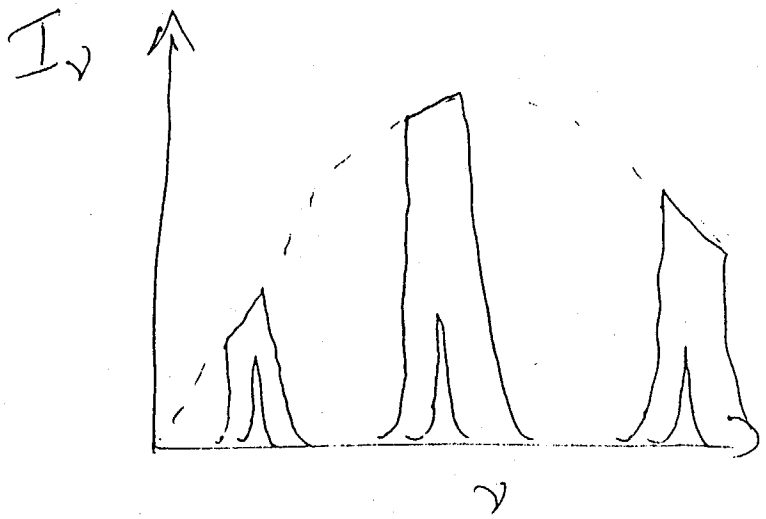

Fig 3

$$f2 = II\,(\pi r_0 hc)^{-1}\,E\,\mu$$

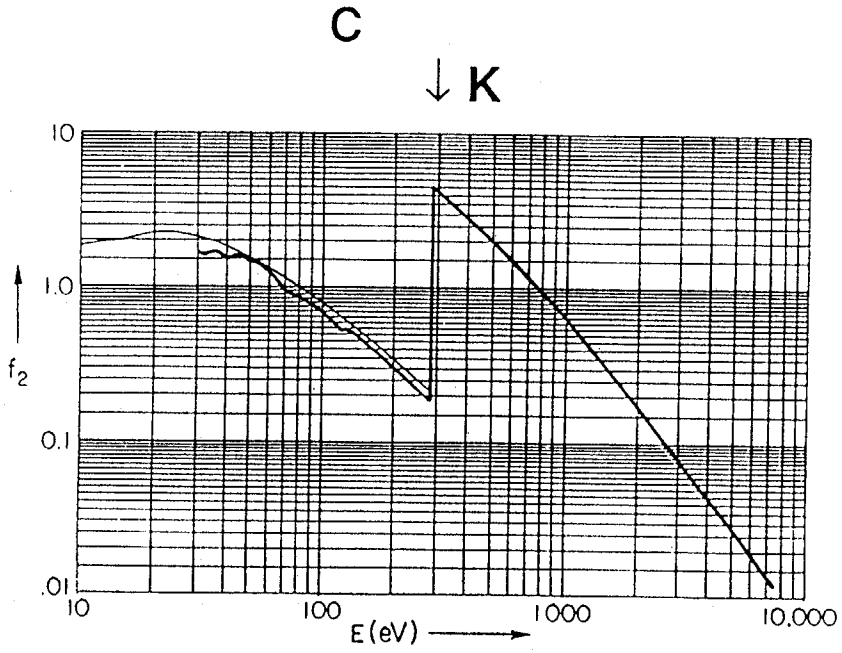

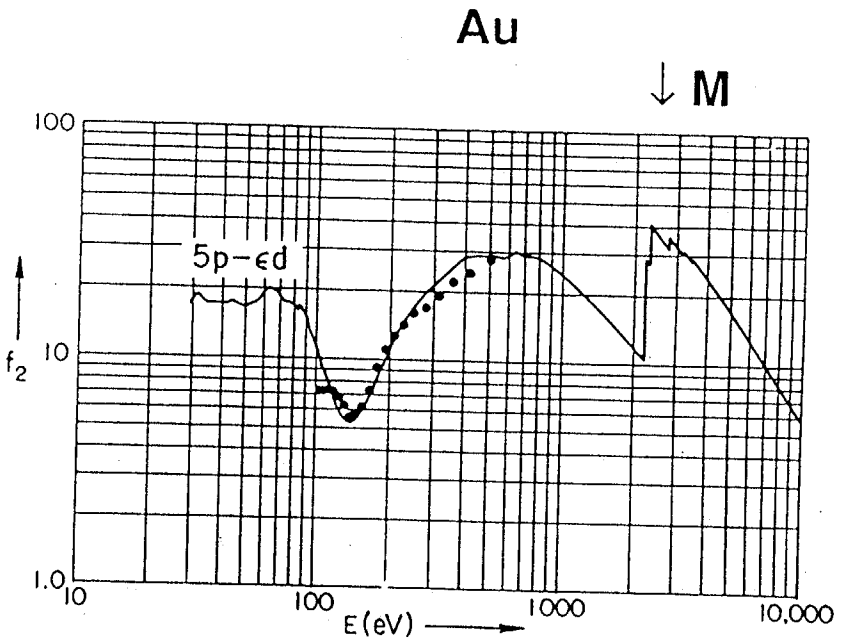

E (kev)	μ/ρ cm²/gm
1.04	4700
2.04	1180
2.29	3680
6.93	314

Figure 4

JDK94-25704

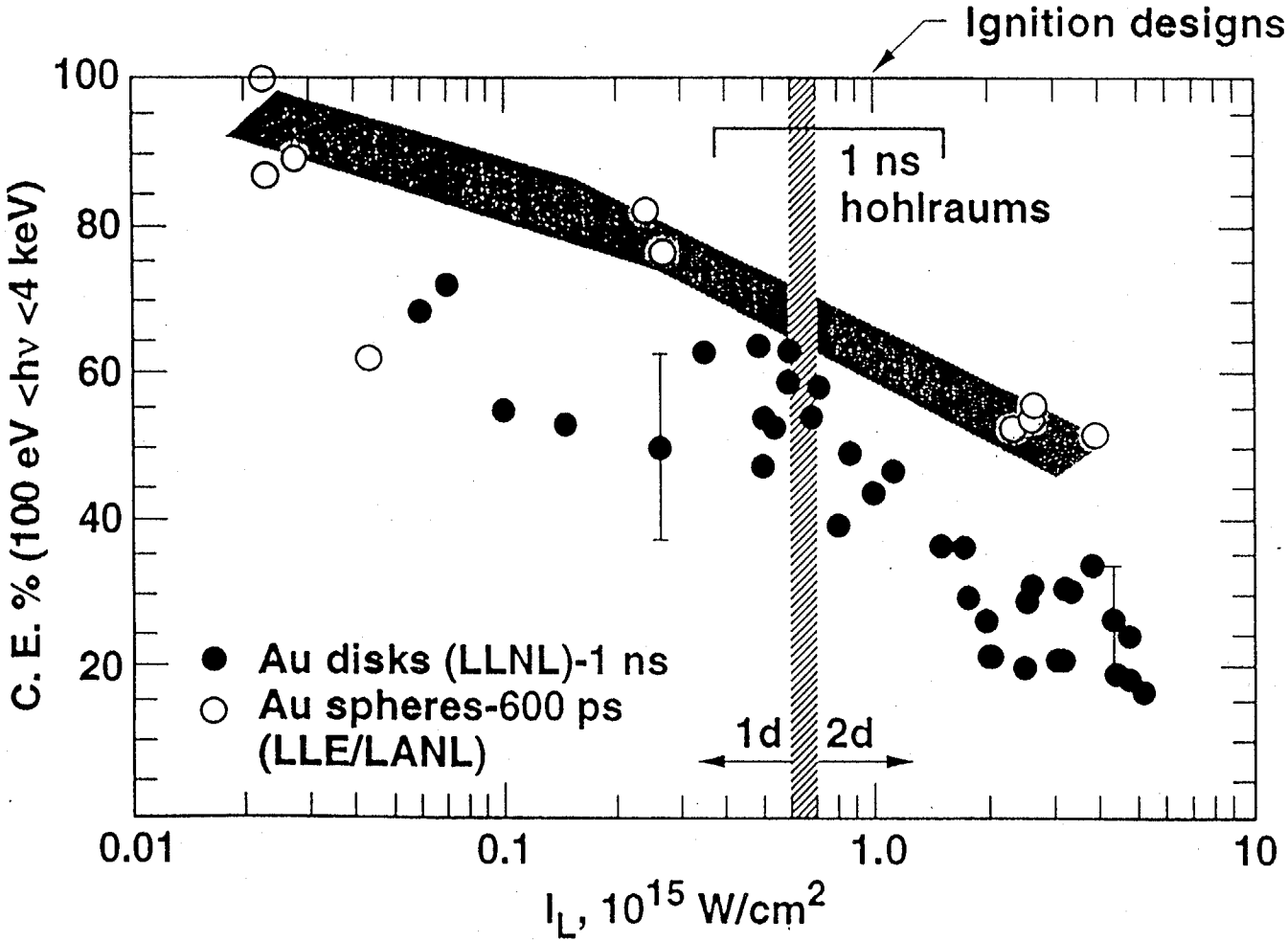

X-ray conversion also increases with pulse length

Figure 5

Au disks
$I \sim 3\text{-}5 \times 10^{14}$ W/cm^2
$\lambda \approx 0.35\mu$

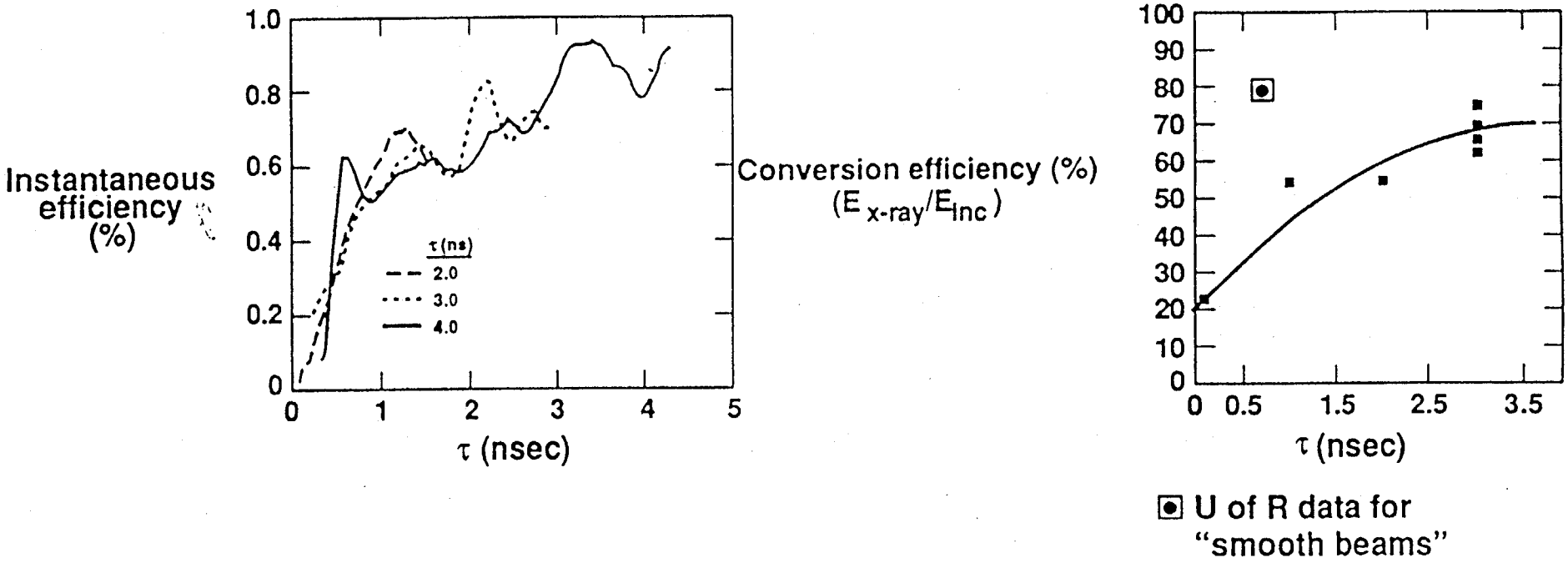

Figure 6

SXI streak image

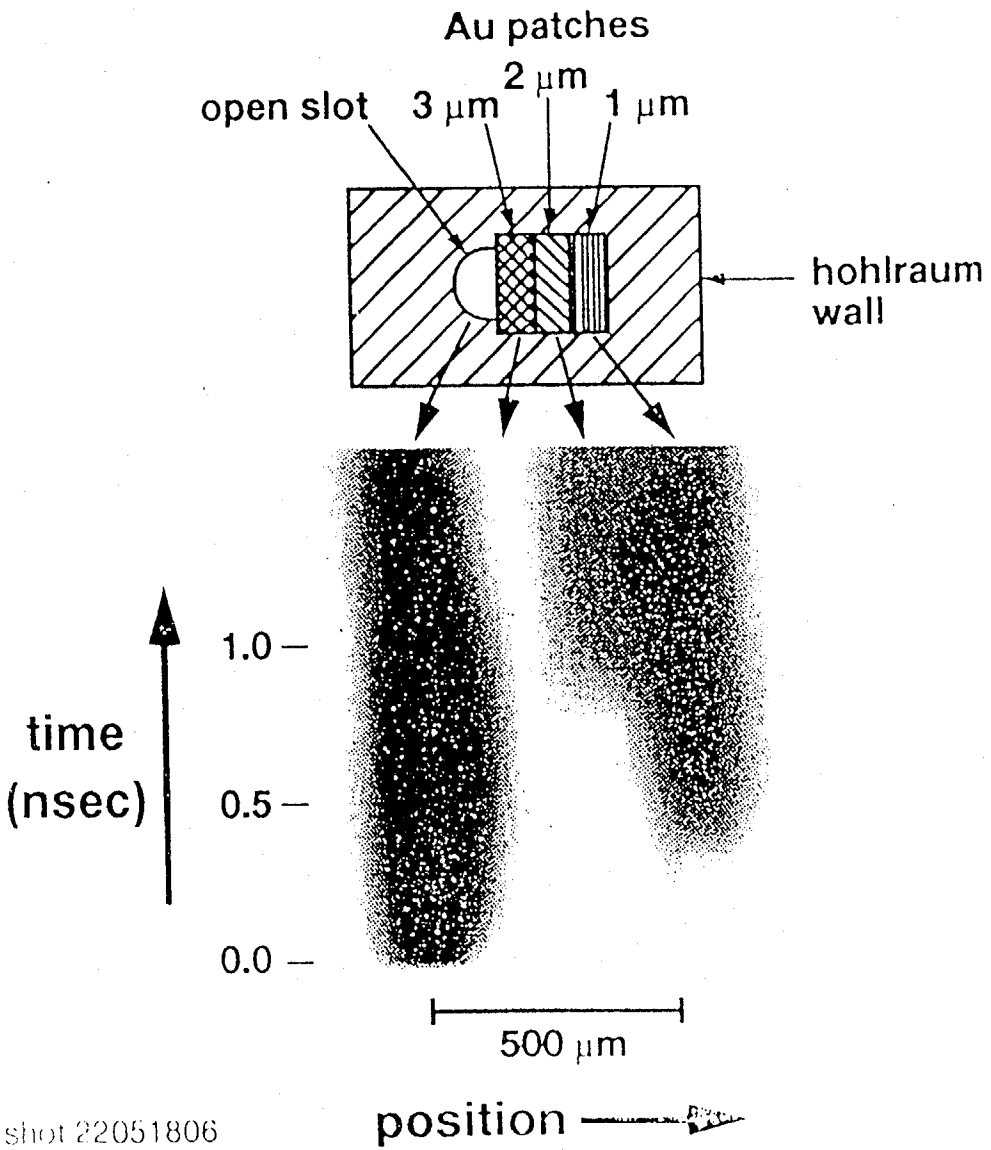

SXI lineout data for Nova shot 22051806

SXI sensitive to hν between 500 and 600

hohlraum: scale 1, 50% LEH

laser: 26 kJ, 3ω, 1-nsec square pulse
(T_r = 260 eV)

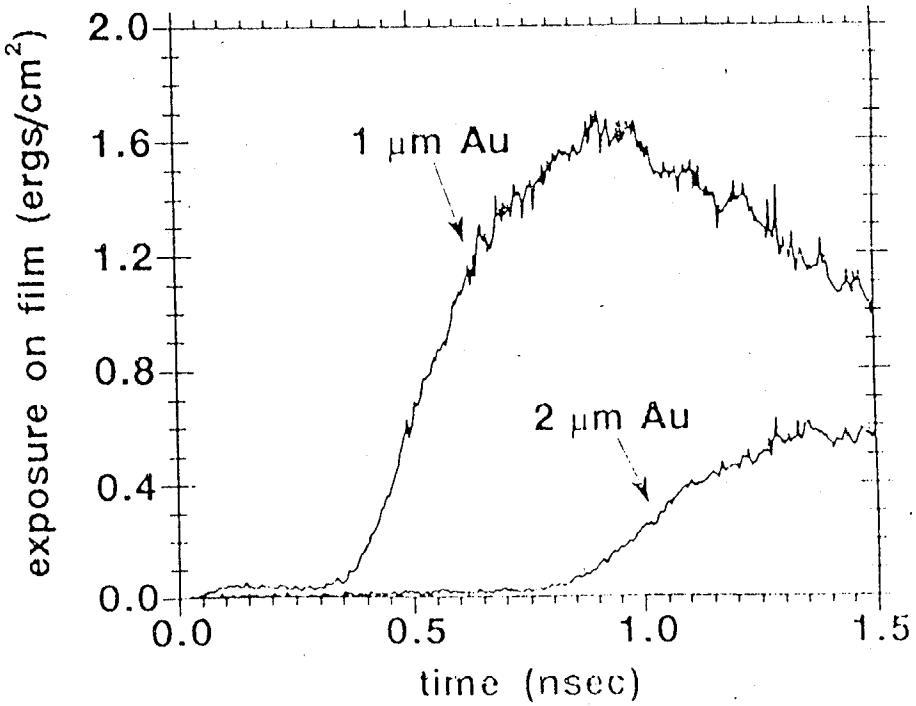

Figure 7

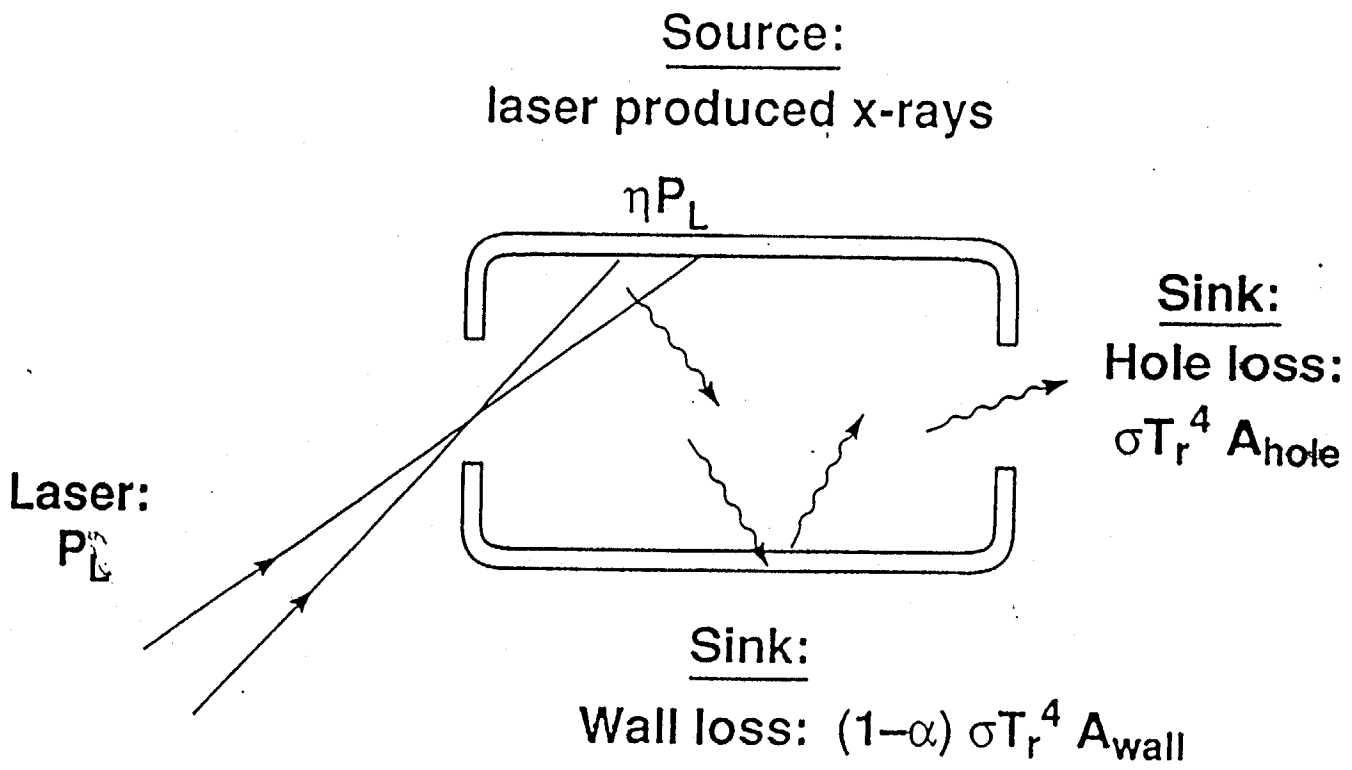

Key parameters: η: Laser light to x-ray conversion efficiency

α: Wall albedo; $(1-\alpha)$: Wall loss

Figure 8

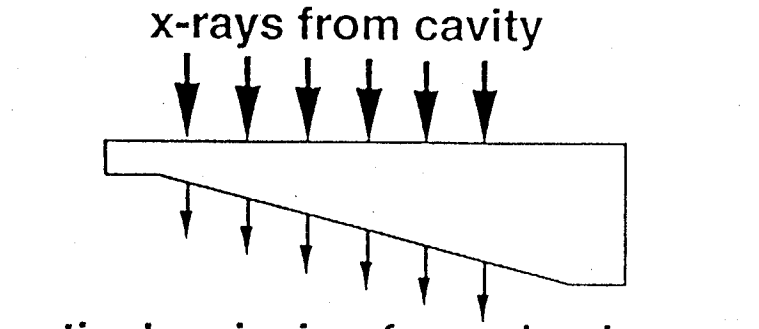
x-rays from cavity
optical emission from shock wave

(a)

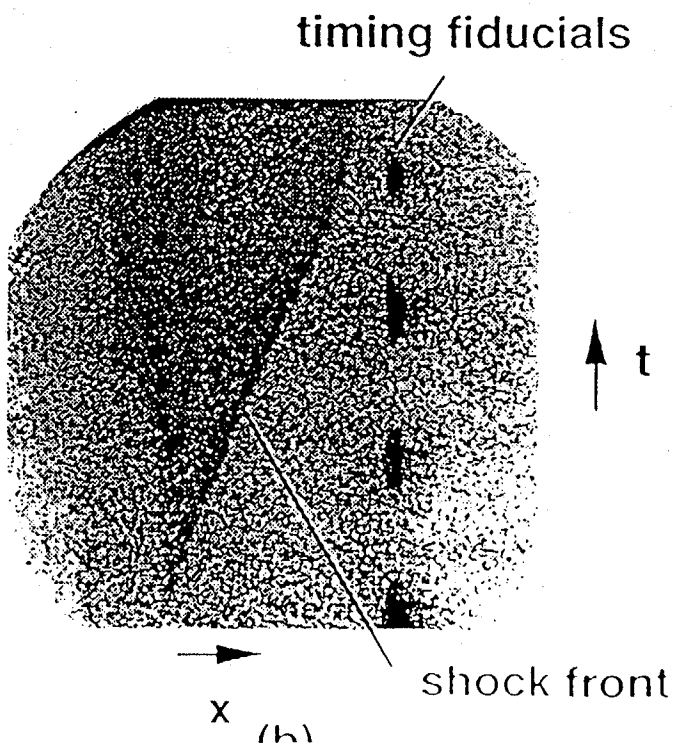
timing fiducials
t
shock front
x

(b)

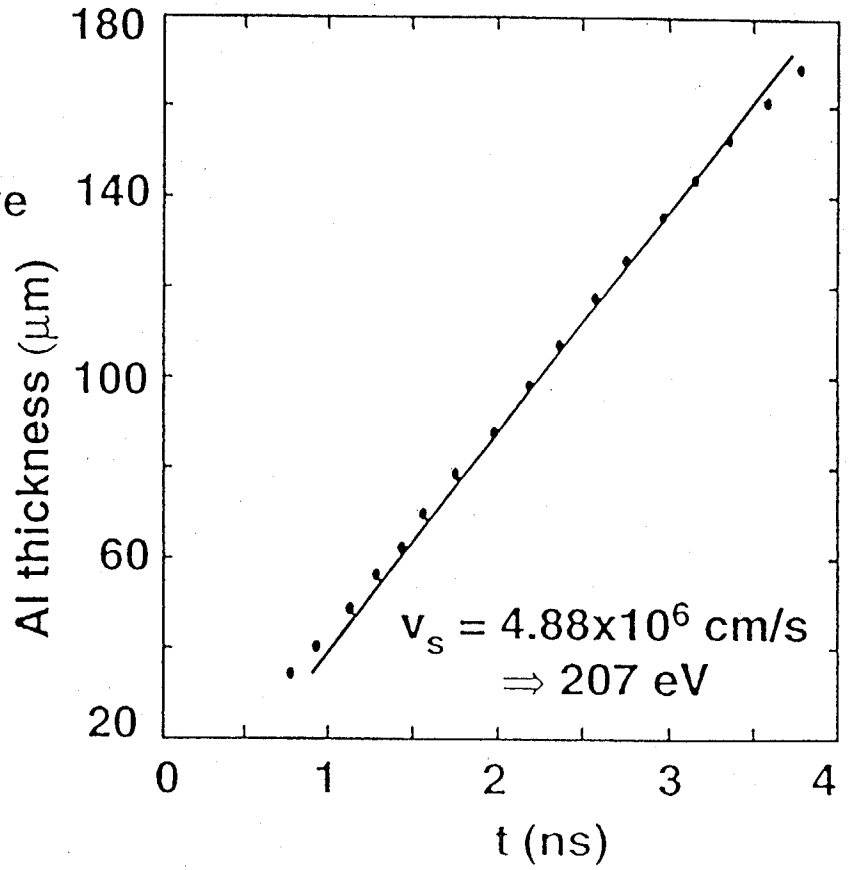
180
140
100
60
20
Al thickness (μm)
0
1
2
3
4
t (ns)
v_s = 4.88x10^6 cm/s
⇒ 207 eV

(c)

Figure 9

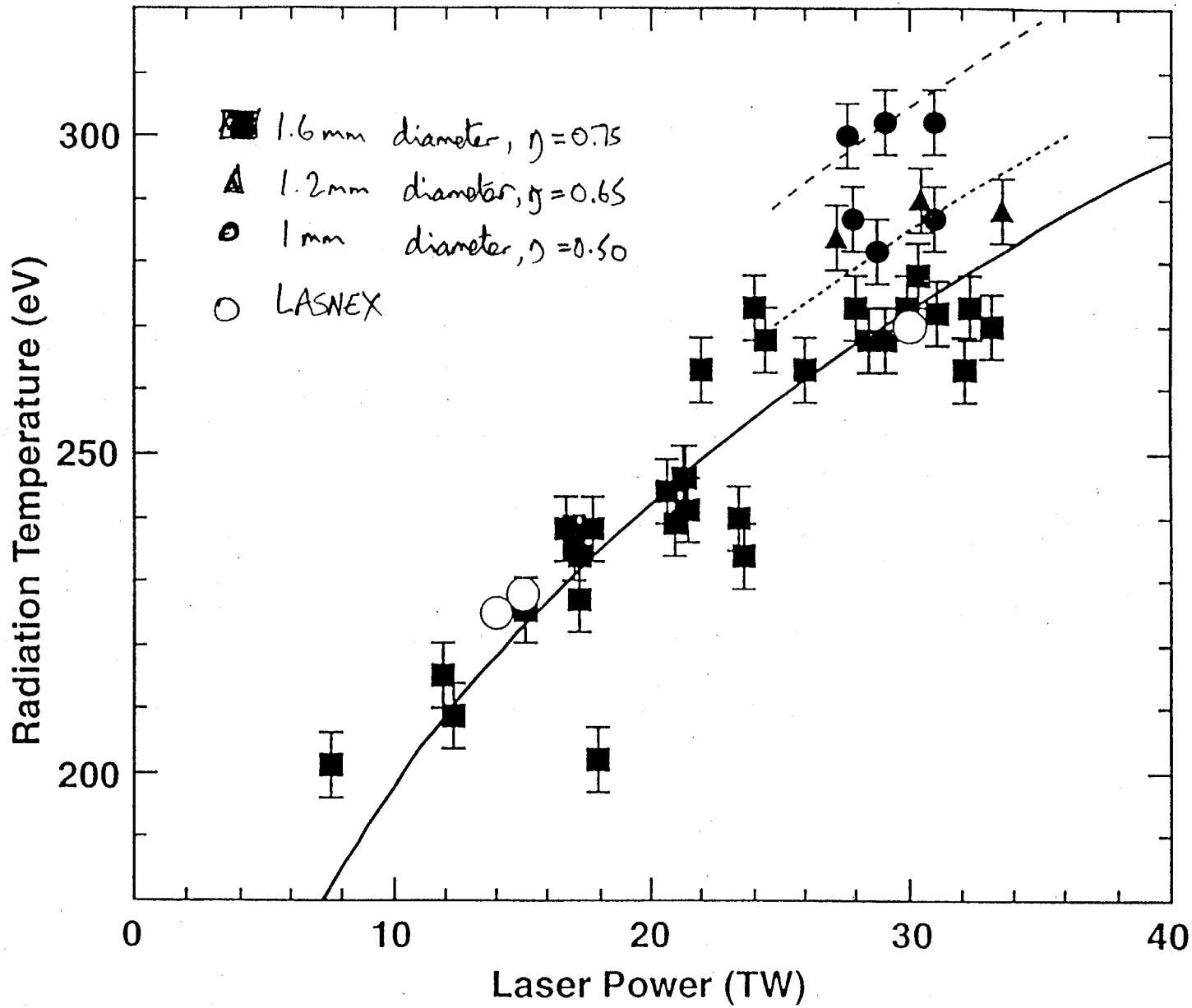
1.6 mm diameter, η=0.75
1.2mm diameter, η=0.65
1 mm diameter, η=0.50
LASNEX
Radiation Temperature (eV)
300
250
200
0
10
20
30
40
Laser Power (TW)

Figure 10

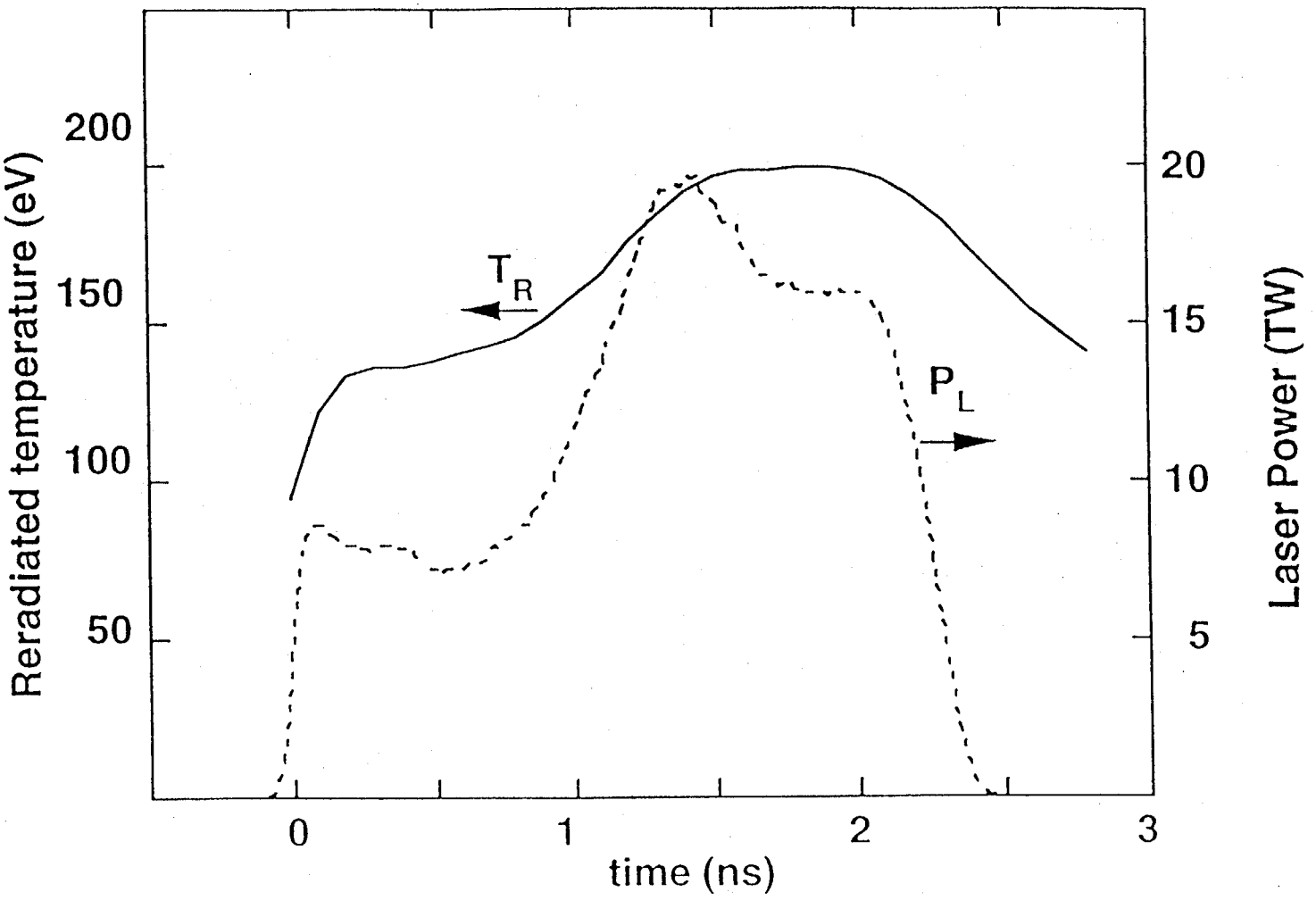
Reradiated temperature (eV)
200
150
100
50
T_R
P_L
20
15
10
5
Laser Power (TW)
0
1
2
3
time (ns)

Figure 11